PNAS RESEARCH ARTICLE | EARTH, ATMOSPHERIC, AND PLANETARY SCIENCES

Industrial-era decline in Arctic methanesulfonic acid is offset by increased biogenic sulfate aerosol

Ursula A. Jongebloed[a,1], Andrew J. Schauer[b], Jihong Cole-Dai[c], Carleigh G. Larrick[c], William C. Porter[d], Linia Tashmim[d], Shuting Zhai[a], Sara Salimi[a], Shana R. Edouard[a], Lei Geng[e], and Becky Alexander[a,1]

Edited by Mark Thiemens, University of California, San Diego, CA; received May 5, 2023; accepted October 17, 2023

Marine phytoplankton are primary producers in ocean ecosystems and emit dimethyl sulfide (DMS) into the atmosphere. DMS emissions are the largest biological source of atmospheric sulfur and are one of the largest uncertainties in global climate modeling. DMS is oxidized to methanesulfonic acid (MSA), sulfur dioxide, and hydroperoxymethyl thioformate, all of which can be oxidized to sulfate. Ice core records of MSA are used to investigate past DMS emissions but rely on the implicit assumption that the relative yield of oxidation products from DMS remains constant. However, this assumption is uncertain because there are no long-term records that compare MSA to other DMS oxidation products. Here, we share the first long-term record of both MSA and DMS-derived biogenic sulfate concentration in Greenland ice core samples from 1200 to 2006 CE. While MSA declines on average by 0.2 μg S kg^{-1} over the industrial era, biogenic sulfate from DMS increases by 0.8 μg S kg^{-1}. This increasing biogenic sulfate contradicts previous assertions of declining North Atlantic primary productivity inferred from decreasing MSA concentrations in Greenland ice cores over the industrial era. The changing ratio of MSA to biogenic sulfate suggests that trends in MSA could be caused by time-varying atmospheric chemistry and that MSA concentrations alone should not be used to infer past primary productivity.

sulfate | phytoplankton | ice core | primary productivity | dimethyl sulfide

Dimethyl sulfide (DMS) from marine phytoplankton is a dominant source of sulfate aerosol in the marine boundary layer (1). After emission to the atmosphere, DMS is oxidized through a complex system of gas-, aqueous-, and multi-phase reactions to form methanesulfonic acid (MSA), sulfur dioxide (SO_2), and hydroperoxymethyl thioformate (HPMTF). These intermediate products can be deposited to the Earth's surface or further oxidized to sulfate (SO_4^{2-}) (2–4). Additionally, these products are an important source of cloud condensation nuclei, and DMS precursor emissions are one of the largest sources of uncertainty in estimating aerosol radiative forcing (5, 6).

To investigate whether and how much marine primary productivity has changed over time, ice core records of MSA concentration are used as a proxy for DMS emissions (7–12). Due to the coincident timing of peak DMS production with the onset of sea ice melt in spring, ice core records of MSA are also used as proxies for sea ice extent (13–17). These ice core MSA records are viewed as robust signals of DMS emissions because there is no other known natural or anthropogenic source of MSA (11). Importantly, MSA is well preserved in high accumulation ice core sites, although migration of the methanesulfonate ion in the ice can smooth seasonal to subdecadal signals (18).

Recently, declining industrial-era MSA concentrations since 1850 were observed in twelve Greenland ice cores and attributed to a decline in North Atlantic primary productivity due to slowing Atlantic Meridional Overturning Circulation (7) or a decline in Arctic sea ice extent (19). More recent Greenland ice core observations show an increasing trend in MSA concentrations from 2000 to 2015, and this trend has been attributed to increasing primary productivity due to earlier Arctic sea ice retreat (12). These somewhat contradictory studies, as well as preceding decades of research, assume that the relative yield of MSA from DMS oxidation is constant over time; however, different oxidation pathways of DMS have different production yields of MSA, and anthropogenic activity has altered emissions of precursors and thus the concentrations of several key oxidants since the preindustrial, including nitrogen oxides (NO_x) (20–23), ozone (24, 25), and reactive halogens such as bromine monoxide and the chlorine radical (19, 26, 27). Thus, confidence in MSA's role as a proxy for DMS emissions has been questioned due to potential changes in the partitioning of MSA, SO_2, and sulfate during DMS oxidation (28).

Sulfate and its precursors (i.e., mainly SO_2 and HPMTF) are the major products of DMS oxidation, but ice core sulfate is not used for investigating DMS emissions because DMS is not the only source of sulfate. Other sulfate sources to the Arctic and global

Significance

Decreasing methanesulfonic acid (MSA) concentrations across Greenland ice cores have suggested declining North Atlantic phytoplankton abundance, with implications for ocean ecosystems and climate. MSA is used to infer phytoplankton abundance because phytoplankton emits dimethyl sulfide (DMS), which is oxidized to MSA and sulfate. However, atmospheric chemistry controls how much DMS is converted to MSA vs. sulfate. Here, we measure DMS-derived sulfate compared to MSA in a Greenland ice core over the industrial era. We show that total biogenic sulfur, the sum of MSA and DMS-derived sulfate, is relatively steady over the industrial era, but MSA declines because anthropogenic pollution affects the ratio of MSA vs. DMS-derived sulfate. Therefore, interpreting MSA as a proxy for DMS emissions must consider atmospheric chemistry.

Author contributions: A.J.S., J.C.-D., L.G., and B.A. designed research; U.A.J., A.J.S., J.C.-D., C.G.L., and B.A. performed research; U.A.J., A.J.S., C.G.L., W.C.P., L.T., S.Z., S.S., S.R.E., and B.A. contributed new reagents/analytic tools; U.A.J., A.J.S., J.C.-D., C.G.L., W.C.P., L.T., S.Z., S.S., S.R.E., and B.A. analyzed data; and U.A.J. and B.A. wrote the paper.

The authors declare no competing interest.

This article is a PNAS Direct Submission.

[1]To whom correspondence may be addressed. Email: ujongebl@uw.edu or beckya@uw.edu.

This article contains supporting information online at https://www.pnas.org/lookup/suppl/doi:10.1073/pnas.2307587120/-/DCSupplemental.

Published November 17, 2023.

atmosphere include volcanic degassing, sea salt, and anthropogenic sources, including fossil fuel combustion and metal smelting (29). Here, we leverage the distinct isotopic composition of DMS-derived biogenic sulfur compared to that of other sources (30–35) to quantify the contribution of DMS to total sulfate in a central Greenland ice core covering 1200 to 2006 CE. We compare this DMS-derived biogenic sulfate to measurements of MSA from the same ice core samples to assess MSA's utility as a proxy for DMS emissions and to examine trends in DMS-derived biogenic sulfur aerosol over this time period.

Results

We measure concentrations of MSA and sulfate (SO_4^{2-}) and sulfur isotopes ($\delta^{34}S$) of sulfate in ice core samples from 1200 to 2006 CE (*Materials and Methods*). Sulfur isotopes are used to estimate the relative contribution from each of the main sources of Arctic sulfate: DMS, volcanic, and anthropogenic emissions (30–35). The influence of sea salt is subtracted from the sulfate concentration and sulfur isotope measurements (*Materials and Methods*). In the preindustrial samples, when the anthropogenic contribution to sulfate concentrations is negligible, we assume that preindustrial non-sea salt sulfate ($nssSO_4^{2-}$) is a sum of biogenic and volcanic sulfate (Eq. **1**) and that $\delta^{34}S(nssSO_4^{2-})$ is a weighted average of the isotopic signatures of sulfate from biogenic ($\delta^{34}S_{bio}$) and volcanic ($\delta^{34}S_{volc}$) sources (Eq. **2**):

$$f_{bio} + f_{volc} = 1, \quad [1]$$

$$f_{bio}\delta^{34}S_{bio} + f_{volc}\delta^{34}S_{volc} = \delta^{34}S\left(nssSO_4^{2-}\right), \quad [2]$$

where the isotopic signatures are estimated to be $\delta^{34}S_{bio}$ = +18.8 ± 0.3‰ and $\delta^{34}S_{volc}$ = +4.1 ± 0.5‰ [*SI Appendix*, Fig. S4 and *Supplementary Text S3*, (34)], and f_{bio} is the biogenic sulfur fraction and f_{volc} is the volcanic sulfur fraction. The concentration of biogenic sulfate is calculated in each sample ($bioSO_4 = f_{bio} \cdot nssSO_4^{2-}$).

In the post-1850 samples, we assume that $nssSO_4^{2-}$ is a sum of anthropogenic, biogenic, and volcanic sulfate (Eq. **3**) and that $\delta^{34}S(nssSO_4^{2-})$ results from a weighted average of $\delta^{34}S_{anthro}$, $\delta^{34}S_{bio}$, and $\delta^{34}S_{volc}$ (Eq. **4**):

$$f_{anth} + f_{bio} + f_{volc} = 1, \quad [3]$$

$$f_{anthro}\delta^{34}S_{anthro} + f_{bio}\delta^{34}S_{bio} + f_{volc}\delta^{34}S_{volc} = \delta^{34}S\left(nssSO_4^{2-}\right), \quad [4]$$

where f_{anthro} is the fraction of anthropogenic sulfate in the sample and $\delta^{34}S_{anthro}$ is the anthropogenic sulfur isotopic source signature, which is estimated to be +2.9 ± 0.3‰ [*SI Appendix, Supplementary Text S3*, (35)]. We assume that source signatures ($\delta^{34}S_{bio}$, $\delta^{34}S_{volc}$, and $\delta^{34}S_{anthro}$) are relatively constant over time (*SI Appendix, Supplementary Text S3*).

The isotopic source signatures of volcanic, DMS-derived biogenic, and anthropogenic sulfur are determined via two methods described in detail in Jongebloed et al. (34, 35) and *SI Appendix, Supplementary Text S3*. The first method is a Keeling Plot, which is the regression of $\delta^{34}S(nssSO_4^{2-})$ measurements against the reciprocal of the concentration measurements ($1/[nssSO_4^{2-}]$) (36–38) and is used to determine $\delta^{34}S_{volc}$ and $\delta^{34}S_{anthro}$ (*SI Appendix*, Fig. S4 *B* and *D*). The Keeling Plot is the preferred method for determining an isotopic source signature because it is only influenced by sulfate sources reaching Summit. The second method is a compilation of direct measurements of DMS-derived sulfur (DMS, DMSP, MSA, and $nssSO_4^{2-}$) for $\delta^{34}S_{bio}$, volcanic sulfur (H_2S, SO_2, and bulk S) for $\delta^{34}S_{volc}$, and anthropogenic sulfur (coal and oil) for $\delta^{34}S_{anthro}$. The global compilations in *SI Appendix*, Fig. S4 *A, C,* and *E* include sources too distant from Greenland to influence the ice core. For this reason, the Keeling Plot determination of sources is used for $\delta^{34}S_{volc}$ and $\delta^{34}S_{anthro}$. The global compilation of DMS-derived sulfur measurements is used for $\delta^{34}S_{bio}$ because DMS-derived sulfur measurements do not vary significantly geographically (39). The comparisons and potential uncertainties in the Keeling Plot regression vs. direct measurement compilation are discussed in *SI Appendix, Supplementary Text S3*.

Possible changes in ice core $\delta^{34}S(nssSO_4^{2-})$ due to changes in DMS and SO_2 oxidation pathways could affect the interpretation of the record in Fig. 1 and thus quantification of $bioSO_4$ and total bioS in Figs. 2 and 3 (40, 41). Previous studies in remote, polar environments suggest that fractionation due to transport and oxidation has a negligible effect on ice core $\delta^{34}S(nssSO_4^{2-})$ (42, 43). Transects of sulfur isotopic composition of sulfate in Antarctica have shown consistent $\delta^{34}S(nssSO_4^{2-})$ values across a geographic region where sources are expected to be nonvarying and thus the only factors influencing $\delta^{34}S(nssSO_4^{2-})$ would be fractionation from transport or oxidation (42, 43). The consistent $\delta^{34}S(nssSO_4^{2-})$ values indicate that fractionation during transport or from oxidation across these scales is a negligible factor influencing $\delta^{34}S(nssSO_4^{2-})$. Additionally, the Keeling Plot determination of source signatures ($\delta^{34}S_{volc}$ and $\delta^{34}S_{anthro}$, *SI Appendix*, *Supplementary Text S3* and Fig. S4) is applied to ice core samples with sulfate that have already been oxidized and transported to the ice sheet, and possible fractionation due to oxidation and transport is inherently included in this method of source signature determination.

Changes in isotopic composition due to changes in fractionation during DMS oxidation are more difficult to constrain. To our knowledge, there is no laboratory quantification of sulfate fractionation caused by different DMS oxidation pathways. However, the similarity in $\delta^{34}S$ between DMSP, DMS, MSA, and DMS-derived $nssSO_4^{2-}$ suggests minimal fractionation (34). Future modeling and laboratory studies should quantify how changes in DMS and SO_2 oxidation could cause fractionation and affect $\delta^{34}S(nssSO_4^{2-})$ and consequently $bioSO_4$ and total bioS.

Fig. 1 shows $nssSO_4^{2-}$ concentration and $\delta^{34}S(nssSO_4^{2-})$ in ice core samples from 1200 to 2006 CE. The concentration of $nssSO_4^{2-}$ triples from the preindustrial mean of 9.6 ± 5.5 μg S kg^{-1} (mean + SD) to a peak concentration of 35.6 ± 7.1 μg S kg^{-1} between 1970 and 1980 (Fig. 1*A*), aligning with previous observations (45). Between 1970 and the top of the core, $nssSO_4^{2-}$ concentration declines to a mean of 12.9 ± 2.8 μg S kg^{-1} from 1996 through 2006. The pattern in $nssSO_4^{2-}$ concentration is mirrored by $\delta^{34}S(nssSO_4^{2-})$, which decreases from +9.2 ± 1.4‰ in the preindustrial to a low of +4.9 ± 0.6‰ from the 1970s through the late 1990s and then increases to +6.6 ± 0.6‰ from 1996 to 2006 (Fig. 1*B*). The trends in $\delta^{34}S(nssSO_4^{2-})$ reflect a shift from natural sulfur sources in the preindustrial ($\delta^{34}S_{bio}$ = +18.8 ± 0.3‰ and $\delta^{34}S_{volc}$ = +4.1 ± 0.5‰) to varying influence of anthropogenic sulfur ($\delta^{34}S_{anthro}$ = +2.9 ± 0.3‰), causing a decreasing and then increasing trend in ice core $\delta^{34}S(nssSO_4^{2-})$ as anthropogenic emissions increase through the 1970s and then decrease following implementation of clean air policies.

Fig. 1*C* shows the fraction of $nssSO_4^{2-}$ concentrations attributable to anthropogenic, volcanic, and DMS-derived biogenic sulfur emissions, which are calculated using $\delta^{34}S(nssSO_4^{2-})$ and Eqs. **1**–**4**. The uncertainty range in the isotopic source signatures for $\delta^{34}S_{volc}$ and $\delta^{34}S_{anthro}$ is calculated using the SE of Keeling Plot intercepts as well as the prediction interval of the Keeling Plot regression (*SI Appendix*, *Supplementary Text S3* and Fig. S6). DMS-derived biogenic fraction of $nssSO_4^{2-}$ (f_{bio}) is 34 ± 9% (mean + SD) of

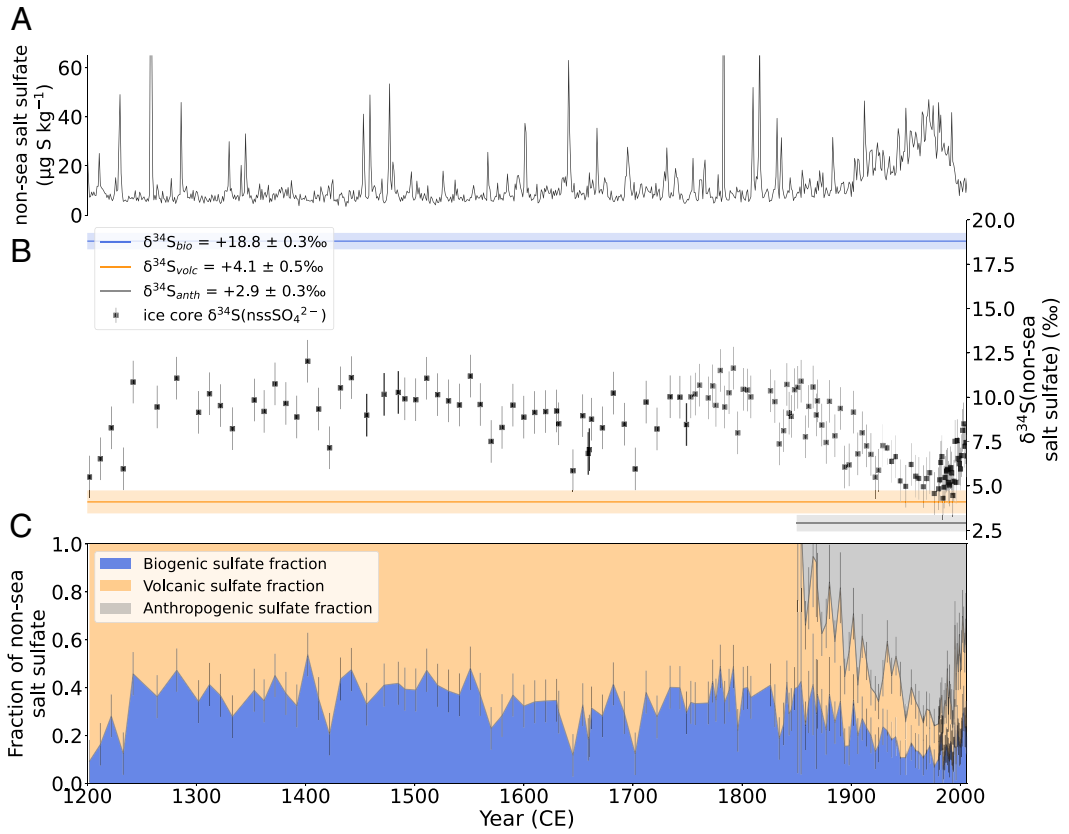

Fig. 1. Ice core measurements of sulfate concentration, sulfur isotopes, and changing sulfur sources from 1200 to 2006 CE. Measurements in ice core samples from Summit, Greenland of (*A*) non-sea salt sulfate concentrations ($nssSO_4^{2-}$ μg S kg^{-1}), (*B*) sulfur isotopic composition ($\delta^{34}S$) of nonsea salt sulfate (‰) with colored lines indicating specific isotopic composition of anthropogenic (gray), biogenic (blue), and volcanic (orange) sources, and (*C*) fraction of nonsea salt sulfate attributed to DMS-derived biogenic sulfate (blue), volcanic sulfate (orange), and anthropogenic sulfate using Eqs. **1**–**4**. Error in the $\delta^{34}S$ measurements, determined by replicate analysis of whole-process standards, is ±1.2‰ (SD). Error in fraction of $nssSO_4^{2-}$ attributed to different sulfur sources is estimated by propagation of measurement error (*SI Appendix, Supplementary Text S1*) and uncertainty in source signatures (*SI Appendix, Supplementary Text S3*).

$nssSO_4^{2-}$ during the preindustrial and f_{bio} decreased as anthropogenic sulfur emissions increased. During the years of maximum anthropogenic sulfur emissions (1972 to 1981) (44), the mean f_{bio} is 12 ± 5%. Clean air policies in North America and Europe reduced anthropogenic sulfur emissions after 1975 (44). As a result, the relative importance of biogenic sulfate increases to f_{bio} = 25 ± 4% of total $nssSO_4^{2-}$ by 2002 to 2006.

Fig. 2 shows the concentration of MSA and biogenic sulfate, which are both oxidation products of DMS, in ice core samples from 1200 to 2006 CE. MSA concentration (Fig. 2*A*) is on average 0.72 ± 0.22 μg S kg^{-1} during the preindustrial. Beginning around 1850, MSA concentration declines by 0.04 μg S kg^{-1} per decade until the late twentieth century. The negative trend in MSA concentration from 1850 to 1996 is statistically significant ($p < 0.01$) and consistent with declining MSA concentrations observed in other Greenland ice cores (7). The minimum MSA concentration is 0.32 ± 0.05 μg S kg^{-1} between 1969 and 1995 CE (*SI Appendix*, Fig. S1), a decrease of 55% from the preindustrial. Around the turn of the century, MSA concentration increases to an average of 0.50 ± 0.24 μg S kg^{-1} between 1996 and 2006 CE (Fig. 1*C*), a trend that is also consistent with a recent Greenland ice core (12).

Fig. 2*B* shows the concentration of $bioSO_4$ and total bioS (MSA + $bioSO_4$) from 1200 to 2006 CE. The $bioSO_4$ concentration increases by 23% from the preindustrial mean of 3.2 ± 1.0 μg S kg^{-1} to a mean concentration of 4.0 ± 1.4 μg S kg^{-1} from 1850 to 2006 CE. The 0.8 ± 0.20 μg S kg^{-1} increase in $bioSO_4$ concentration is greater than the 0.19 ± 0.36 μg S kg^{-1} decrease in MSA from the preindustrial to the industrial shown in Fig. 2*A*. As a result of an increase in $bioSO_4$ concentration that is larger than the decrease in industrial-era MSA concentration, total bioS (MSA + $bioSO_4$) concentration is 17% higher ($p < 0.01$) in the industrial era (4.6 ± 1.4 μg S kg^{-1}) relative to the preindustrial (3.9 ± 1.1 μg S kg^{-1}).

The uncertainty in isotopic source signatures contributes to uncertainty in $bioSO_4$ and total bioS concentration. For example, if $\delta^{34}S_{bio}$, $\delta^{34}S_{volc}$, and $\delta^{34}S_{anthro}$ are determined from the compilation of direct measurements from only the back trajectory region (45° N to 90° N, 120° W to 30° E; back-trajectory mean shown as dashed lines in *SI Appendix*, Fig. S4 *A*, *B*, and *D*), the change in total bioS from the preindustrial to the industrial era is 3.6 to 4.0 μg S kg^{-1} (an increase of 13%), whereas the change in total bioS from the preindustrial to the industrial era from the global compilation of $\delta^{34}S_{bio}$ and Keeling Plot determination of $\delta^{34}S_{volc}$ and $\delta^{34}S_{anthro}$ is 3.9 to 4.6 μg S kg^{-1} (an increase of 17%). The increase of 13% vs. 17% is similar because $\delta^{34}S_{bio}$ is very distinct from $\delta^{34}S_{volc}$ and $\delta^{34}S_{anthro}$. Additionally, we note that both mean estimates (3.6 vs. 3.9 μg S kg^{-1} in the preindustrial era and 4.0 vs. 4.6 μg S kg^{-1} in the industrial era) are within the uncertainty range (± 1.4 μg S kg^{-1}) shown as error bars in Fig. 3*B*.

MSA is a minor component of total bioS throughout the record (Figs. 2*D* and 3*A*). During the preindustrial (1200 to 1850 CE), MSA is 19 ± 5% of total bioS (Figs. 2*D* and 3*A*), then declines to 8 ± 3% during the MSA minimum from 1969 to 1995 and increases to 13 ± 5% of total bioS in the last 10 y of the record (Figs. 2*D* and 3*A*). $BioSO_4$ is the major oxidation product of DMS emissions and the main component of total bioS from 1200 to 1850 (81 ± 5%), 1969 to 1995 (92 ± 3%), and 1996 to 2006

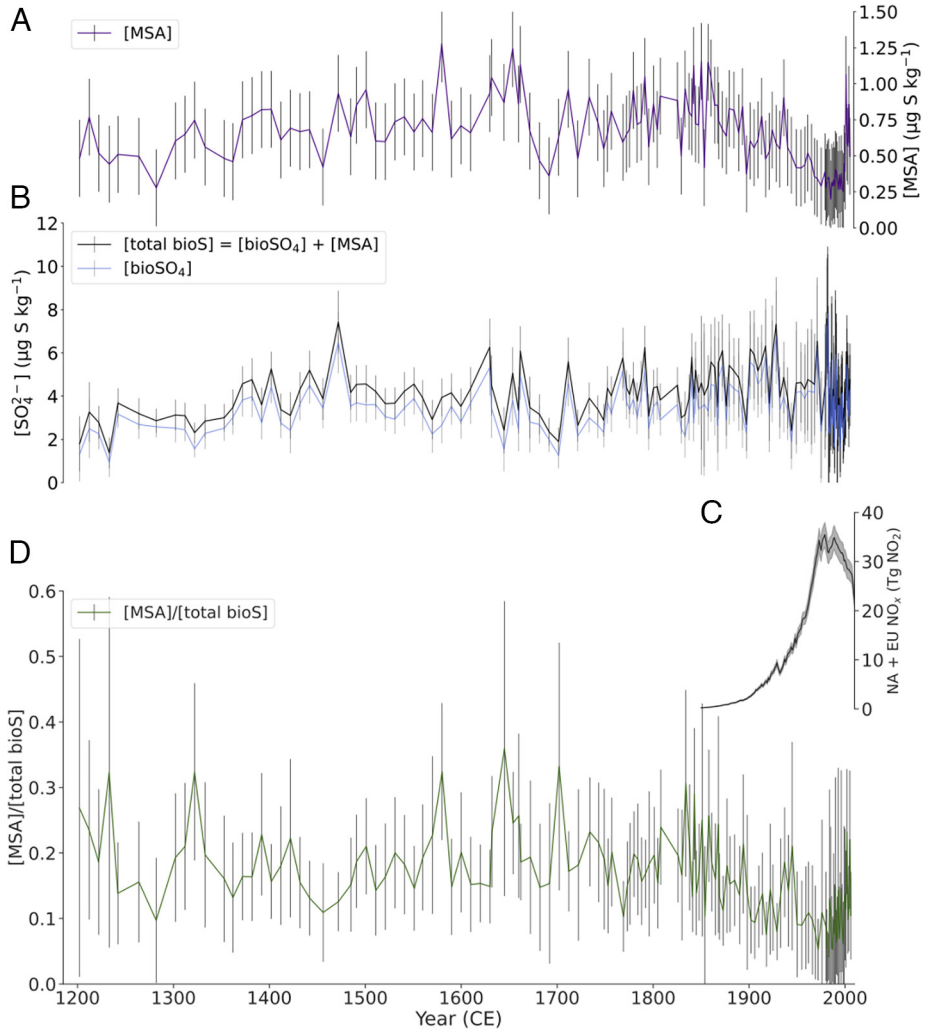

Fig. 2. Concentrations of DMS-derived sulfur species in ice core samples from Summit, Greenland from 1200 to 2006 CE. (*A*) MSA (μg S kg^{-1}), where the detection limit for MSA is estimated with replicate measurement to be 0.03 μg S kg^{-1}. (*B*) bioSO$_4$ (μg S kg^{-1}) and total bioS (MSA + bioSO$_4$) (μg S kg^{-1}). (*C*) Annual emissions of NO_x ($NO + NO_2$, Tg NO_2 y^{-1}) from North America plus Europe from 1850 to 2010 from the Community Emissions Data System (CEDS) inventory (44), with shaded range based on reported 1-sigma uncertainty estimate. (*D*) Ratio of MSA to total bioS in ice core samples from Summit, Greenland from 1200 to 2006 CE. Error in the biogenic sulfate concentrations, total biogenic sulfur concentrations, and MSA to total bioS ratio are determined with the propagation of uncertainty in isotopic source signatures (*SI Appendix, Supplementary Text S3*) and sample measurement error (*SI Appendix, Supplementary Text S1*).

(87 ± 5%). The higher total bioS concentrations during the MSA minimum (4.4 ± 1.8 μg S kg^{-1}) and present day (4.0 ± 1.2 μg S kg^{-1}) relative to the preindustrial (3.9 ± 1.1 μg S kg^{-1}) (Fig. 2*B*) suggests that the DMS source of sulfur aerosol has not decreased since the preindustrial, but the relative yield of MSA vs. sulfate from DMS oxidation has changed (Figs. 2*D* and 3*A*).

Assuming a constant ratio of MSA to total bioS results in erroneous assumed trends in DMS-derived total sulfur aerosol in the Arctic and North Atlantic atmosphere over the industrial era. Fig. 3*B* demonstrates the difference between the observed ("true") total bioS anomaly (relative to the observed preindustrial mean) and what the assumed ("false") total bioS anomaly would be assuming [MSA]/[total bioS] is constant over the industrial era. The assumed normalized total bioS is calculated by multiplying the normalized preindustrial total bioS concentrations by the percent change in MSA concentrations between the preindustrial and shown time periods. The assumed total bioS during the MSA minimum (1969 to 1995), present day (1996 to 2006), and industrial era (1850 to 2006) is statistically significantly lower (60%, 31%, and 37%, respectively; $p < 0.01$) than the observed normalized total bioS during the same time periods. The difference between observed and assumed total bioS illustrates the flaw in assuming that MSA concentrations are a robust proxy for DMS emissions and total DMS-derived sulfur aerosol.

Discussion

The observed changes in ice core [MSA]/[total bioS] suggest changes in the relative yield of MSA vs. sulfate production from the oxidation of DMS. The ratio of DMS oxidation products is dependent on environmental conditions such as temperature, concentration of different oxidants, and the presence of clouds (3, 4, 46–48). The DMS oxidation mechanism involves both gas- and multi-phase chemistry, and different oxidants favor different DMS oxidation products. The most important oxidation pathways of DMS are thought to be gas-phase oxidation by the hydroxyl radical (OH) during the daytime (50 to 60%), which occurs by hydrogen abstraction and addition, and by the nitrate radical (NO_3) during the nighttime (15 to 35%) (49, 50). Other DMS oxidants include bromine monoxide (BrO, 8 to 29%), the chlorine radical (Cl, 4 to 10%), and ozone (O_3) in the gas and aqueous phases (2 to 8%) (49, 50).

Using MSA as a proxy for primary productivity assumes that the oxidation chemistry of DMS has remained relatively constant over long time periods; however, with the possible exception of

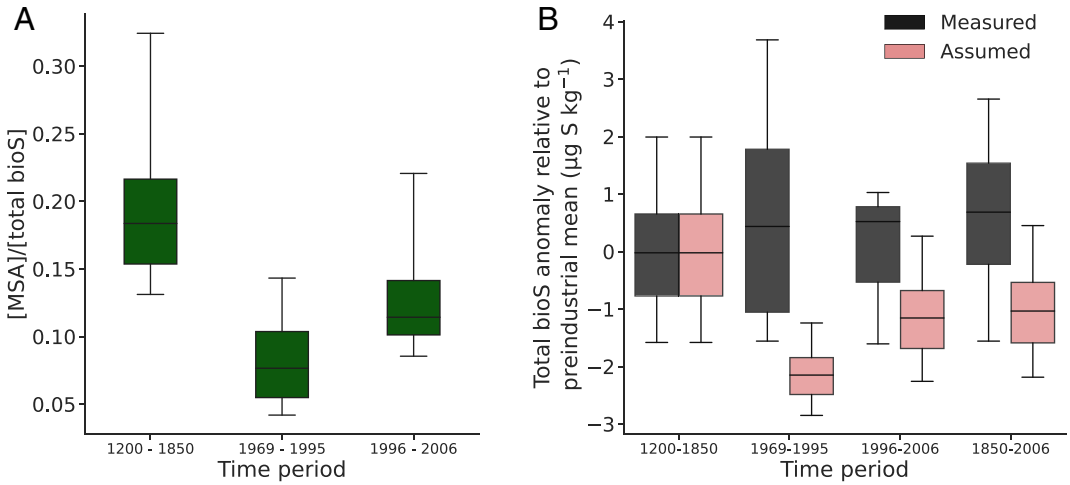

Fig. 3. [MSA]/[total bioS] and comparison in measured vs. assumed total bioS over different time periods. (*A*) Comparison of measured [MSA]/[total bioS] (green) over the preindustrial (74 samples representing 123 y between 1200 and 1850), MSA minimum (18 samples representing 18 y between 1969 and 1995), and present day (11 samples representing 11 y between 1996 to 2006). (*B*) Comparison of measured total bioS (black) vs. what the assumed total bioS would be if total bioS decreased by the same factor as MSA (pink) over the same time periods shown in (*A*) and over the industrial era (1850 to 2006 CE). Measured and assumed total bioS are both shown as an anomaly in concentration relative to the mean preindustrial (1200 to 1850) concentration. Boxes represent median and interquartile range and whiskers represent the 5th and 95th percentile.

OH, the abundance of all other DMS oxidants has changed due to anthropogenic emissions. In particular, emissions of NO_x, which are precursors to the nitrate radical (NO_3), increased from the preindustrial to 1970, remained elevated from 1970 to 1990, and then declined in the early 21st century [Fig. 2*C*; (20–22)] in regions affecting the Summit air-mass source region that includes eastern North America and western Europe (26).

DMS oxidation by NO_3 is one of the main loss processes of DMS and favors the production of SO_2 and HPMTF over MSA (50). All else being equal, elevated NO_3 concentrations will increase the partitioning of DMS toward the SO_2 and HPMTF oxidation pathway. The increase in NO_x emissions from 1850 to the 1970s coincides with the decline in MSA concentration (Fig. 2 *C* and *D* and *SI Appendix*, Fig. S1). As NO_x emissions decreased after 1990 (Fig. 2*C*), DMS oxidation shifted back toward the MSA oxidation pathway, as reflected in the increased [MSA]/[total bioS] at the end of the record (0.13 ± 0.05 from 1996 to 2006) relative to the [MSA]/[total bioS] during the MSA minimum (0.08 ± 0.03 from 1969 to 1995) (Fig. 2*C*) and increase in MSA concentration (*SI Appendix*, Fig. S1). This hypothesis is supported by atmospheric chemistry modeling by Fung et al. (50), which showed that the DMS + NO_3 oxidation pathway is less important during the preindustrial due to lower NO_x emissions, and even with modeling the same DMS emissions in the preindustrial and present-day, global MSA burden is 59% higher in the preindustrial compared to the present day.

DMS oxidation chemistry is complex, and it is possible that reactions other than the DMS + NO_3 pathway could have contributed to or partially offset the industrial-era decline in MSA. For example, MSA destruction through aqueous and heterogeneous oxidation by OH could convert up to 75% of MSA to sulfate (50, 51) and could have increased in efficiency in the twentieth century due to increased cloud droplet acidity (52). Reactive halogens are DMS oxidants that have been perturbed by anthropogenic activities, including BrO (27) and Cl (26). Additionally, uncertainty remains in reaction intermediates, particularly HPMTF (48, 53), which has highly uncertain cloud uptake and loss process rates. Thus, changes in cloud properties, such as cloud droplet number concentration influenced by sulfate aerosol, could change oxidation and loss of HPMTF and other sulfur species. Additionally, varying relative humidity, organic peroxy radical concentration, and NO concentration change the relative yield of DMS oxidation products in ways that are not captured by models and require further study (54). Finally, understanding how the oxidation of DMS and other marine biogenic sulfur compounds such as methanethiol (55) have contributed to trends in MSA, SO_2, and SO_4^{2-} production requires further investigation.

The robustness of these conclusions depends on accurate determination of $\delta^{34}S_{bio}$, $\delta^{34}S_{volc}$, and $\delta^{34}S_{anthro}$. The Keeling Plot regressions in *SI Appendix*, Fig. S4 *B* and *D* and compilations of direct measurements in *SI Appendix*, Fig. S4 *B* and *E* provide independent $\delta^{34}S_{volc}$ and $\delta^{34}S_{anthro}$ that are statistically indistinguishable. Although $\delta^{34}S_{bio}$ is determined only by a compilation of direct $\delta^{34}S$ measurements of DMS-derived sulfur compounds (*SI Appendix*, Fig. S4*A*), Amrani et al. (39) find that $\delta^{34}S_{bio}$ does not vary significantly by region. Furthermore, our analysis is qualitatively consistent even when the analysis is performed on a subset of the compilation from measurements only in the back-trajectory region: Total bioS does not decrease over the industrial era despite the decrease in industrial-era MSA concentrations (*SI Appendix, Supplementary Text S3D*).

We note that despite the increase in [MSA]/[total bioS] in 1996 to 2006 relative to 1969 to 1995 (Figs. 2 *D* and 3*A*), which reduces the relative yield of sulfate produced from DMS, f_{bio} increases from ~1975 to 2006 due to decreasing anthropogenic sulfur emissions (Fig. 1*C*). As anthropogenic sulfur emissions decrease, the magnitude of anthropogenic sulfate aerosol cooling decreases (56), and the relative abundance and radiative importance of natural sulfate sources, including DMS, increases.

Conclusions

Our ice core measurements of biogenic sulfate ($bioSO_4$) and MSA concentrations from 1200 to 2006 CE show that MSA concentrations declined from 1850 CE through the late twentieth century, while $bioSO_4$ is higher in the industrial relative to the preindustrial. The cause for the decline in MSA is likely changing DMS oxidation chemistry from changes in atmospheric concentrations of key oxidants, including the nitrate radical, which increases the relative yield of SO_2 and sulfate from oxidation of DMS (49). Although more investigation is required to quantify the effects of atmospheric chemistry on MSA and sulfate, our results show that relative yield of MSA from oxidation of DMS is variable over time and that MSA

alone is not a reliable proxy for oceanic DMS emissions. Uncertainty in how changing sulfur isotope fractionation due to changing DMS and SO_2 oxidation pathways over the industrial era affects interpretation of $\delta^{34}S(nssSO_4^{2-})$ also requires future investigation. Overall, total bioS and $bioSO_4$ concentrations throughout the ice core record suggest that industrial era DMS emissions are not significantly lower than, and possibly even slightly higher than, DMS emissions during the preindustrial. This finding contradicts previous studies inferring industrial-era primary productivity decline from observed ice core MSA concentrations (7, 12).

Since the preindustrial, anthropogenic sulfate has had a net cooling effect on the atmosphere (57), but as anthropogenic emissions of SO_2 decrease, the cooling effect of anthropogenic sulfate is diminished (56). As a result, biogenic sulfate will become a relatively more important source of cloud concentration nuclei and potentially more important to Earth's radiative balance. Assuming anthropogenic sulfur emissions will continue to decrease in the future (58), perturbations in biogenic sulfur could have a relatively larger role in Earth's climate. Understanding how DMS emission have changed and will change in the future relies on robust proxies for primary productivity, which requires understanding of how changing atmospheric chemistry affects the interpretation of these proxies.

Materials and Methods

We measure MSA concentration, sulfate concentration, and sulfur isotopic composition of sulfate [$\delta^{34}S(SO_4^{2-})$] in samples from a Summit, Greenland ice core in years between 1200 and 2006 CE without influence from large volcanic eruptions (59, 60). Detailed methods for sample selection and analysis are described by Jongebloed et al. (34, 35) and in *SI Appendix, Supplementary Text S1*. We analyzed a total of 135 samples representing 184 sampled years, including one sample per decade from 1200 to 1750 CE at 2-y resolution, one sample every 4 y from 1750 to 1980 CE at 1-y resolution, and one sample each year at 1-y resolution from 1980 to 2006 CE. The aim of the sampling scheme is to quantify preindustrial (1200 to 1850 CE) biogenic sulfate ($bioSO_4$) and MSA concentrations compared to recent decades. The uncertainty for sample $\delta^{34}S(SO_4^{2-})$ measurement determined by replicate analysis of whole-process standards is ±1.20‰. The fraction of sea salt sulfate (f_{ss}) and non-sea salt sulfate ($nssSO_4^{2-}$) in each sample is calculated using the mass fraction of bulk sea water $SO_4^{2-}/Na^+ = 0.25$ (61) and isotopic signature of sea salt sulfate ($\delta^{34}S_{ss} = +21‰$; (62).

The similar isotopic signatures of volcanic and anthropogenic sulfur prevent clear separation of volcanic and anthropogenic sulfate in post-1850 samples. We therefore assume the industrial-era volcanic sulfate concentrations ($[volcSO_4]_{assumed}$) are equal to the preindustrial median and subtract this from the non-sea salt sulfate concentration and isotopic composition of non-sea salt sulfate (Eqs. **5** and **6**):

$$\left[nssSO_4^{2-}\right] - \left[volcSO_4\right]_{assumed} = \left[bioSO_4\right] + \left[anthroSO_4\right], \quad [5]$$

$$\delta^{34}S\left(nssSO_4^{2-}\right) - f_{volc,\,assumed}\delta^{34}S_{volc} = f_{anthro}\delta^{34}S_{anthro} + f_{bio}\delta^{34}S_{bio}. \quad [6]$$

We also subtract a range of volcanic sulfate concentrations ±2 SDs around the mean preindustrial volcanic sulfate concentration to investigate a range of possible solutions, such that $[volcSO_4]_{assumed,\ 97.5th\ percentile} = X + 2\sigma$ and $[volcSO_4]_{assumed,\ 2.5th\ percentile} = X - 2\sigma$, where X and σ are the mean and SD, respectively, of the preindustrial volcanic sulfate concentrations. We attribute the remaining sulfate to biogenic and anthropogenic sulfur and determine the concentration of biogenic sulfate in each sample. The range in $[volcSO_4]_{assumed}$ is shown in *SI Appendix*, Fig. S2 and the resulting range in $[bioSO_4]$ is shown in *SI Appendix*, Fig. S3. The wide range in assumed volcanic sulfate concentrations contributes only 28% of the uncertainty (total uncertainty = ± 1.4 μg kg^{-1}) in estimated biogenic sulfate concentrations because the isotopic signature of biogenic sulfur is distinct from the anthropogenic and volcanic signatures.

Sulfur isotopic source signatures for biogenic ($\delta^{34}S_{bio}$), volcanic ($\delta^{34}S_{volc}$), and anthropogenic ($\delta^{34}S_{anthro}$) sulfur emissions are determined through Keeling Plot regressions and compilations of $\delta^{34}S$ measurements from direct source gas emissions, described in detail in Jongebloed et al. (34, 35), *SI Appendix, Supplementary Text S3* and Fig. S4. We assume that these source signatures are consistent over the preindustrial and industrial eras (*SI Appendix, Supplementary Text S3*). This assumption is supported by consistency between Keeling Plot determinations of source signatures with source signatures determined by compilations of measurements representing different regions and time periods (*SI Appendix, Supplementary Text S3*). However, the effects of possible changes in fractionation effects on $\delta^{34}S(nssSO_4^{2-})$ due to changing oxidation pathways of DMS and SO_2 must be investigated in future work to quantify how this might affect the quantification of $bioSO_4$ from ice core $\delta^{34}S(nssSO_4^{2-})$. A larger uncertainty range based on the prediction interval of the Keeling Plot regression is shown for the $bioSO_4$ and total bioS concentrations in *SI Appendix*, Fig. S6.

Ice core samples for MSA measurement were prepared following established decontamination procedures (63). MSA concentrations were measured using a Sciex QTRAP 5500 tandem mass spectrometer. The mass spectrometric measurement method is similar to that used in previous studies of MSA in ice cores (64) and an internal standard (deuterated MSA) was used for quantitation. The detection limit for MSA is estimated with replicate measurement to be 0.03 μg S kg^{-1}. To calculate the total biogenic sulfur (total bioS), we add ice core MSA concentration (μg S kg^{-1}) and biogenic sulfate concentration (μg S kg^{-1}).

Data, Materials, and Software Availability. All ice core data are available in the NSF Arctic Data Center at https://doi.org/10.18739/A2WW7717K, https://doi.org/10.18739/A2N873162, and https://doi.org/10.18739/A26T0GX7K (65–67). All study data are included in the article and/or *SI Appendix*.

ACKNOWLEDGMENTS. U.A.J. and B.A. acknowledge NSF Division of Polar Programs (PLR) grants 1904128, 629363, and Atmospheric and Geospace Sciences (AGS) 1702266. J.C-D. acknowledges NSF grants PLR 0612461, PLR 1904142, and PLR 2230351. L.G. acknowledges the support from National Natural Science Foundation of China (41822605 and 41871051). W.C.P. and L.T. acknowledge NSF grant AGS 2155192.

Author affiliations: [a]Department of Atmospheric Sciences, University of Washington, Seattle, WA 98195; [b]Department of Earth and Space Sciences, University of Washington, Seattle, WA 98195; [c]Department of Chemistry and Biochemistry, South Dakota State University, Brookings, SD 57007; [d]Department of Environmental Science, University of California, Riverside, CA 92521; and [e]Deep Space Exploration Laboratory, School of Earth and Space Sciences, University of Science and Technology of China, Hefei, Anhui, China 230052

1. M. O. Andreae, Ocean-atmosphere interactions in the global biogeochemical sulfur cycle. *Mar. Chem.* **30**, 1–29 (1990).
2. A. R. Ravishankara, Heterogeneous and multiphase chemistry in the troposphere. *Science* **276**, 1058–1065 (1997).
3. I. Barnes, J. Hjorth, N. Mihalopoulos, Dimethyl sulfide and dimethyl sulfoxide and their oxidation in the atmosphere. *Chem. Rev.* **106**, 940–975 (2006).
4. E. H. Hoffmann *et al.*, An advanced modeling study on the impacts and atmospheric implications of multiphase dimethyl sulfide chemistry. *Proc. Natl. Acad. Sci. U.S.A.* **113**, 11776–11781 (2016).
5. K. S. Carslaw *et al.*, Large contribution of natural aerosols to uncertainty in indirect forcing. *Nature* **503**, 67–71 (2013).
6. A. Gettelman, Putting the clouds back in aerosol-cloud interactions. *Atmos. Chem. Phys.* **15**, 12397–12411 (2015).
7. M. B. Osman *et al.*, Industrial-era decline in subarctic Atlantic productivity. *Nature* **569**, 551–555 (2019).
8. D. J. Polashenski *et al.*, Denali ice core methanesulfonic acid records North Pacific marine primary production. *J. Geophys. Res. Atmos.* **123**, 4642–4653 (2018).
9. E. S. Saltzman, I. Dioumaeva, B. D. Finley, Glacial/interglacial variations in methanesulfonate (MSA) in the Siple Dome ice core, West Antarctica. *Geophys. Res. Lett.* **33**, 26649–26657 (2006).
10. E. S. Saltzman, P. Y. Whung, P. A. Mayewski, Methanesulfonate in the Greenland ice sheet project 2 ice core. *J. Geophys. Res. Oceans* **102**, 26649–26657 (1997).
11. M. Legrand, P. Mayewski, Glaciochemistry of polar ice cores: A review. *Rev. Geophys.* **35**, 219–243 (1997).
12. Y. Kurosaki, S. Matoba, Y. Iizuka, K. Fujita, R. Shimada, Increased oceanic dimethyl sulfide emissions in areas of sea ice retreat inferred from a Greenland ice core. *Commun. Earth Environ.* **3**, 327 (2022).
13. E. C. Osterberg *et al.*, Coastal ice-core record of recent northwest Greenland temperature and sea-ice concentration. *J. Glaciol.* **61**, 1137–1146 (2015).
14. N. J. Abram, R. Mulvaney, C. Arrowsmith, Environmental signals in a highly resolved ice core from James Ross Island, Antarctica. *J. Geophys. Res. Atmos.* **116**, D20116 (2011).

15. N. J. Abram, E. W. Wolff, M. A. J. Curran, A review of sea ice proxy information from polar ice cores. *Quat. Sci. Rev.* **79**, 168–183 (2013).
16. M. A. J. Curran *et al.*, Post-depositional movement of methanesulphonic acid at Law Dome, Antarctica, and the influence of accumulation rate. *Ann. Glaciol.* **35**, 333–339 (2002).
17. M. A. J. Curran, T. D. van Ommen, V. I. Morgan, K. L. Phillips, A. S. Palmer, Ice core evidence for Antarctic Sea ice decline since the 1950s. *Science* **302**, 1203–1206 (2003).
18. M. Osman, S. B. Das, O. Marchal, M. J. Evans, Methanesulfonic acid (MSA) migration in polar ice: Data synthesis and theory. *Cryosphere* **11**, 2439–2462 (2017).
19. O. J. Maselli *et al.*, Sea ice and pollution-modulated changes in Greenland ice core methanesulfonate and bromine. *Climate of the Past* **13**, 39–59 (2017).
20. M. T. Lund *et al.*, Concentrations and radiative forcing of anthropogenic aerosols from 1750 to 2014 simulated with the Oslo CTM3 and CEDS emission inventory. *Geosci. Model. Dev.* **11**, 4909–4931 (2018).
21. D. A. Hauglustaine, Y. Balkanski, M. Schulz, A global model simulation of present and future nitrate aerosols and their direct radiative forcing of climate. *Atmos. Chem. Phys.* **14**, 11031–11063 (2014).
22. L. Xu, J. E. Penner, Global simulations of nitrate and ammonium aerosols and their radiative effects. *Atmos. Chem. Phys.* **12**, 9479–9504 (2012).
23. H. Wang *et al.*, Increased night-time oxidation over China despite widespread decrease across the globe. *Nat. Geosci.* **16**, 217–223 (2023), 10.1038/s41561-022-01122-x.
24. A. Gaudel *et al.*, Tropospheric ozone assessment report: Present-day distribution and trends of tropospheric ozone relevant to climate and global atmospheric chemistry model evaluation. *Elementa* **6**, 39 (2018).
25. L. Y. Yeung *et al.*, Isotopic constraint on the twentieth-century increase in tropospheric ozone. *Nature* **570**, 224–227 (2019).
26. S. Zhai *et al.*, Anthropogenic impacts on tropospheric reactive chlorine since the preindustrial. *Geophys. Res. Lett.* **48**, e2021GL093808 (2021).
27. T. Sherwen *et al.*, Global impacts of tropospheric halogens (Cl, Br, I) on oxidants and composition in GEOS-Chem. *Atmos. Chem. Phys.* **16**, 12239–12271 (2016).
28. M. Legrand *et al.*, Sulfur-containing species (methanesulfonate and SO4) over the last climatic cycle in the Greenland Ice Core Project (central Greenland) ice core. *J. Geophys. Res. Oceans* **102**, 26663–26679 (1997).
29. J. P. D. Abbatt *et al.*, Overview paper: New insights into aerosol and climate in the Arctic. *Atmos. Chem. Phys.* **19**, 2527–2560 (2019).
30. V. Wasiuta, A.-L. Norman, S. Marshall, Spatial patterns and seasonal variation of snowpack sulphate isotopes of the Prince of Wales Icefield, Ellesmere Island, Canada. *Ann. Glaciol.* **43**, 390–396 (2006).
31. R. Ghahremaninezhad, A. L. Norman, J. P. D. Abbatt, M. Levasseur, J. L. Thomas, Biogenic, anthropogenic and sea salt sulfate size-segregated aerosols in the Arctic summer. *Atmos. Chem. Phys.* **16**, 5191–5202 (2016).
32. N. Patris *et al.*, First sulfur isotope measurements in central Greenland ice cores along the preindustrial and industrial periods. *J. Geophys. Res. Atmos.* **107**, ACH 6-1–ACH 6-11 (2002).
33. A. L. Norman *et al.*, Sources of aerosol sulphate at Alert: Apportionment using stable isotopes. *J. Geophys. Res.* **104**, 11619–11631 (1999).
34. U. A. Jongebloed *et al.*, Underestimated passive volcanic sulfur degassing implies overestimated anthropogenic aerosol forcing. *Geophys. Res. Lett.* **50**, e2022GL102061 (2023).
35. U. A. Jongebloed *et al.*, Sulfur isotopes quantify the impact of anthropogenic activities on industrial-era Arctic sulfate in a Greenland ice core. *Environ. Res. Lett.* **18**, 074020 (2023). 10.1088/1748-9326/acdc3d.
36. D. E. Pataki *et al.*, The application and interpretation of Keeling plots in terrestrial carbon cycle research. *Global Biogeochem. Cycles* **17**, 1022 (2003).
37. C. D. Keeling, The concentration and isotopic abundances of atmospheric carbon dioxide in rural areas. *Geochim. Cosmochim. Acta* **13**, 322 (1958).
38. C. D. Keeling *et al.*, "A three-dimensional model of atmospheric CO2 transport based on observed winds: 1. Analysis of observational data" in *Aspects of Climate Variability in the Pacific and the Western Americas*, D. H. Peterson, Ed. (AGU, 1989), pp. 165–236.
39. A. Amrani, W. Said-Ahmad, Y. Shaked, R. P. Kiene, Sulfur isotope homogeneity of oceanic DMSP and DMS. *Proc. Natl. Acad. Sci. U.S.A.* **110**, 18413–18418 (2013).
40. E. D. Sofen, B. Alexander, S. A. Kunasek, The impact of anthropogenic emissions on atmospheric sulfate production pathways, oxidants, and ice core $\Delta 17O(SO4_{2-})$. *Atmos. Chem. Phys.* **11**, 3565–3578 (2011).
41. E. Harris *et al.*, Sulfur isotope fractionation during oxidation of sulfur dioxide: Gas-phase oxidation by OH radicals and aqueous oxidation by H2O2, O3 and iron catalysis. *Atmos. Chem. Phys.* **12**, 407–424 (2012).
42. R. Uemura *et al.*, Sulfur isotopic composition of surface snow along a latitudinal transect in East Antarctica. *Geophys. Res. Lett.* **43**, 5878–5885 (2016).
43. S. Ishino *et al.*, Homogeneous sulfur isotope signature in East Antarctica and implication for sulfur source shifts through the last glacial–interglacial cycle. *Sci. Rep.* **9**, 12378 (2019).
44. E. E. McDuffie *et al.*, A global anthropogenic emission inventory of atmospheric pollutants from sector- and fuel-specific sources (1970–2017): An application of the Community Emissions Data System (CEDS). *Earth Syst. Sci. Data* **12**, 3413–3442 (2020).
45. P. A. Mayewski *et al.*, Sulfate and nitrate concentrations from a South Greenland Ice Core. *Science* **232**, 975–977 (1986).
46. R. von Glasow, P. J. Crutzen, Model study of multiphase DMS oxidation with a focus on halogens. *Atmos. Chem. Phys.* **3**, 6733–6777 (2004).
47. P. J. Hezel *et al.*, Modeled methanesulfonic acid (MSA) deposition in Antarctica and its relationship to sea ice. *J. Geophys. Res. Atmos.* **116**, D23214 (2011).
48. G. A. Novak *et al.*, Rapid cloud removal of dimethyl sulfide oxidation products limits SO_2 and cloud condensation nuclei production in the marine atmosphere. *Proc. Natl. Acad. Sci. U.S.A.* **118**, e2110472118 (2021).
49. Q. Chen, T. Sherwen, M. Evans, B. Alexander, DMS oxidation and sulfur aerosol formation in the marine troposphere: A focus on reactive halogen and multiphase chemistry. *Atmos Chem. Phys.* **18**, 13617–13637 (2018).
50. K. M. Fung *et al.*, Exploring dimethyl sulfide (DMS) oxidation and implications for global aerosol radiative forcing. *Atmos Chem. Phys.* **22**, 1549–1573 (2022).
51. E. L. Mungall, J. P. S. Wong, J. P. D. Abbatt, Heterogeneous oxidation of particulate methanesulfonic acid by the hydroxyl radical: Kinetics and atmospheric implications. *ACS Earth Space Chem.* **2**, 48–55 (2018).
52. K. C. Kwong *et al.*, Chemical transformation of methanesulfonic acid and sodium methanesulfonate through heterogeneous OH oxidation. *ACS Earth Space Chem.* **2**, 895–903 (2018).
53. P. R. Veres *et al.*, Global airborne sampling reveals a previously unobserved dimethyl sulfide oxidation mechanism in the marine atmosphere. *Proc. Natl. Acad. Sci. U.S.A.* **117**, 4505–4510 (2020).
54. Q. Ye *et al.*, Product distribution, kinetics, and aerosol formation from the OH oxidation of dimethyl sulfide under different RO_2 regimes. *Atmos Chem. Phys.* **22**, 16003–16015 (2022).
55. G. A. Novak, D. B. Kilgour, C. M. Jernigan, M. P. Vermeuel, T. H. Bertram, Oceanic emissions of dimethyl sulfide and methanethiol and their contribution to sulfur dioxide production in the marine atmosphere. *Atmos Chem. Phys.* **22**, 6309–6325 (2022).
56. D. Shindell, G. Faluvegi, Climate response to regional radiative forcing during the twentieth century. *Nat. Geosci.* **2**, 294–300 (2009).
57. G. Myhre *et al.*, Radiative forcing of the direct aerosol effect from AeroCom Phase II simulations. *Atmos Chem. Phys.* **13**, 1853–1877 (2013).
58. S. Szopa *et al.*, "Short-lived climate forcers" in *Climate Change 2021: The Physical Science Basis. Contribution of Working Group I to the Sixth Assessment Report of the Intergovernmental Panel on Climate Change*, V. Masson-Delmotte *et al.*, Eds. (Cambridge University Press, Cambridge, United Kingdom and New York, NY, 2021), pp. 817–922.
59. E. Gautier *et al.*, 2600-years of stratospheric volcanism through sulfate isotopes. *Nat. Commun.* **10**, 466 (2019).
60. J. Cole-Dai *et al.*, Two likely stratospheric volcanic eruptions in the 1450s C.E. found in a bipolar, subannually dated 800 year ice core record. *J. Geophys. Res. Atmos.* **118**, 7459–7466 (2013).
61. H. D. Holland, *The Chemistry of the Atmosphere and Oceans* (Wiley, 1978).
62. C. E. Rees, W. J. Jenkins, J. Monster, The sulphur isotopic composition of ocean water sulphate*. *Geochim. Cosmochim. Acta* **42**, 377–381 (1978).
63. K. Peterson, J. Cole-Dai, D. Brandis, T. Cox, S. Splett, Rapid measurement of perchlorate in polar ice cores down to sub-ngL−1 levels without pre-concentration. *Anal. Bioanal. Chem.* **407**, 7965–7972 (2015).
64. E. S. Saltzman, I. Dioumaeva, B. D. Finley, Glacial/interglacial variations in methanesulfonate (MSA) in the Siple Dome ice core, West Antarctica. *Geophys. Res. Lett.* **33**, 2005GL025629 (2006).
65. U. A. Jongebloed *et al.*, Sulfur isotopes of sulfate measurements from a Greenland ice core (1850–2006). Arctic Data Center (2023), 10.18739/A26T0GX7K.
66. U. A. Jongebloed *et al.*, Methanesulfonic acid measurements from a Greenland ice core (1850–2006). Arctic Data Center (2023), 10.18739/A2WW7717K.
67. U. A. Jongebloed *et al.*, Sulfur isotopes of sulfate measurements from a Greenland ice core (1200-1850) and volcanic gas measurements from various volcanoes and hot springs in Iceland. Arctic Data Center (2023), 10.18739/A2N873162.